

Nucleon Excited States from Lattice QCD and Hamiltonian Effective Field Theory

Jia-jun Wu · Jonathan M. M. Hall · H.
Kamano · Waseem Kamleh · T.-S. H.
Lee · Derek B. Leinweber · Zhan-Wei
Liu · Finn M. Stokes · Anthony W.
Thomas

Received: date / Accepted: date

Abstract An approach for relating the nucleon excited states extracted from lattice QCD and the nucleon resonances of experimental data has been developed using the Hamiltonian effective field theory (HEFT) method. By formulating HEFT in the finite volume of the lattice, the eigenstates of the Hamiltonian model can be related to the energy eigenstates observed in Lattice simulations. By taking the infinite-volume limit of HEFT, information from the lattice is linked to experiment. The approach opens a new window for the study of experimentally-observed resonances from the first principles of lattice QCD calculations. With the Hamiltonian approach, one not only describes the spectra of lattice-QCD eigenstates through the eigenvalues of the finite-volume Hamiltonian matrix, but one also learns the composition of the

Jia-jun Wu
Special Research Centre for the Subatomic Structure of Matter (CSSM),
Department of Physics, University of Adelaide, Adelaide, South Australia 5005, Australia
HISKP (Theory) and BCTP, University of Bonn, Germany
E-mail: jiajun.wu@adelaide.edu.au

Jonathan M. M. Hall, Waseem Kamleh, Derek B. Leinweber, Finn M. Stokes, Anthony W.
Thomas
Special Research Centre for the Subatomic Structure of Matter (CSSM),
Department of Physics, University of Adelaide, Adelaide, South Australia 5005, Australia
ARC Centre of Excellence for Particle Physics at the Terascale (CoEPP),
Department of Physics, University of Adelaide, Adelaide, South Australia 5005, Australia

Zhan-Wei Liu
School of Physical Science and Technology,
Lanzhou University, Lanzhou 730000, China

H. Kamano
KEK Theory Center, Institute of Particle and Nuclear Studies (IPNS), High Energy Accelerator Research Organization (KEK), Tsukuba, Ibaraki 305-0801, Japan
J-PARC Branch, KEK Theory Center, IPNS, KEK, Tokai, Ibaraki 319-1106, Japan

T.-S. H. Lee
Physics Division, Argonne National Laboratory, Argonne, Illinois 60439, USA

lattice-QCD eigenstates via the eigenvectors of the Hamiltonian matrix. One learns the composition of the states in terms of the meson-baryon basis states considered in formulating the effective field theory. One also learns the composition of the resonances observed in Nature. In this presentation, I will focus on recent breakthroughs in our understanding of the structure of the $N^*(1535)$, $N^*(1440)$ and $\Lambda^*(1405)$ resonances using this method.

1 Introduction

The nature of the low lying resonances is one of the most challenging problems in modern hadron physics. It is still hard to understand the spectra of light baryons and mesons within Quantum Chromodynamics (QCD) because of the non-perturbative property. Lattice QCD realizes the non-perturbative calculation based on the Monte Carlo simulation technique in the finite-volume. In recent years, it makes a lot of important progresses [1]. It is therefore necessary to connect the lattice QCD results and experimental data to investigate the resonances. There are various approaches to connect the experimental data and the energy levels in the finite-volume [2, 3, 4, 5, 6, 7, 8, 9, 10, 11, 12, 13, 14, 15, 16].

In this report, the Hamiltonian effective field theory (HEFT) is reviewed based on recent references, [17, 18, 19, 20, 21, 22, 23, 24]. HEFT is an extension of chiral perturbation theory [17, 25]. In the infinite volume, through solving a three-dimensional reduction of the coupled-channel Bethe-Salpeter equation, the Hamiltonian generates the scattering amplitudes, T-matrix, which is straightforward to the experimental observables. On the other hand, through solving a eigen-equation of the finite-volume Hamiltonian matrix, the eigenvalues corresponding to the energy levels of lattice QCD can be obtained. From one Hamiltonian model, we build the relationship between the experimental data and finite-volume energy levels. This relationship is consistent with the model independent formalism developed by Lüscher [2, 3] as proved in Ref.[18]. Although HEFT relies on the Hamiltonian model, the model dependence parts in this relationship are absorbed into the exponential suppressed terms of the lattice size. Furthermore, HEFT also provides the eigenvectors of the eigenstates in the finite-volume. The eigenvectors directly reveal the composition of these eigenstates which carry information on the internal structure of the resonances. Therefore, HEFT provides a unique way to study the inside structure of resonances with experimental and lattice QCD data.

In principle, HEFT requires to measure all eigenstates in the finite-volume, however, current lattice techniques can not arrive this requirement. For the baryon pure three-quark local operators are mostly used, while rarely some calculations use Meson-Baryon non-local operators [26]. In this report, we focus on the results from three-quark local operators. The reasonable assumption is that the state extracted in the finite-volume by three-quark local operators should take a large component of three-quark core. HEFT can be used to examine the three-quark core components of the $N^*(1535)$, $\Lambda^*(1405)$ and

$N^*(1440)$ states [19, 20, 21, 22, 23]. In this report, we review recent results and build a new picture of low lying resonances.

The framework of HEFT is described in Sec. 2. The relationship between the eigenstates in the finite-volume and the resonances are discussed. In Sec.3, the numerical results and discussions of $N^*(1535)$, $\Lambda^*(1405)$ and $N^*(1440)$ are presented. Based on the studies of these resonances, a new picture of the low lying hadron spectrum is proposed. A brief summary concludes in Sec. 4.

2 Framework of HEFT

2.1 The Hamiltonian

In the rest frame, the Hamiltonian has the following form

$$H = H_0 + H_I, \quad (1)$$

where the non-interacting Hamiltonian is

$$H_0 = \sum_{B_0} |B_0\rangle m_B^0 \langle B_0| + \sum_{\alpha} \int d^3\mathbf{k} |\alpha(\mathbf{k})\rangle [\omega_{\alpha_M}(\mathbf{k}) + \omega_{\alpha_N}(\mathbf{k})] \langle \alpha(\mathbf{k})|. \quad (2)$$

Here B_0 denotes a bare baryon with mass m_B^0 , which may be thought of as a quark model state, α designates the channel and α_M (α_N) indicates the meson (baryon) state which constitutes channel α . The energy $\omega_{\alpha_i}(\mathbf{k}) = \sqrt{m_{\alpha_i}^2 + \mathbf{k}^2}$.

The energy independent interaction Hamiltonian includes two parts, $H_I = g + v$, where g describes the vertex interaction between the bare particle and the two-particle channels α

$$g = \sum_{\alpha, B_0} \int d^3\mathbf{k} \left\{ |\alpha(\mathbf{k})\rangle G_{\alpha, B_0}^{\dagger}(k) \langle B_0| + h.c. \right\}, \quad (3)$$

while the direct two-to-two particle interaction is defined by

$$v = \sum_{\alpha, \beta} \int d^3\mathbf{k} d^3\mathbf{k}' |\alpha(\mathbf{k})\rangle V_{\alpha, \beta}^S(k, k') \langle \beta(\mathbf{k}')|. \quad (4)$$

Here we consider three different resonances, $N^*(1535)$, $N^*(1440)$ and $\Lambda^*(1405)$, so different interaction forms and channels for them are involved. For the $N^*(1535)$, it includes πN and ηN channels, and $N^*(1440)$ includes πN , $\pi\Delta$ and σN channels, while it has $\pi\Sigma$, $\bar{K}N$, $\eta\Lambda$, $K\Xi$ and $\pi\Lambda$ channels for $\Lambda^*(1405)$.

For the vertex interaction between the bare baryon and the two-particle channels we choose:

$$G_{\alpha, B_0}^2(k) = \frac{3 g_{B_0\alpha}^2}{4 \pi^2 f^2} \omega_{\alpha_1}(k) u^2(k), \quad (5)$$

for $N^*(1535)$ and $\Lambda^*(1405)$ case, where the pion decay constant $f = 92.4$ MeV and the form factor is chosen as $u(k) = (1 + k^2/\Lambda^2)^{-2}$, and $\Lambda = 0.8$ and 1.0 GeV for $N^*(1535)$ and $\Lambda^*(1405)$, respectively. For the $N^*(1440)$ case, we choose:

$$G_{\alpha, B_0}^2(k) = \frac{g_{B_0\alpha}^2}{4\pi^2} \left(\frac{k}{f}\right)^{2l_\alpha} \frac{u_\alpha^2(k)}{\omega_{\alpha 1}(k)}, \quad (6)$$

where l_α is the orbital angular momentum in channel α . Here, since we are concerned with the Roper resonance, with isospin, angular momentum and parity, $\mathbf{I}(\mathbf{J}^P) = \frac{1}{2}(\frac{1}{2}^+)$, l is 1 for πN and $\pi\Delta$, while it is 0 for σN . The regulating form factor, $u_\alpha(k)$, takes the exponential form $u_\alpha(k) = \exp(-k^2/\Lambda_\alpha^2)$, where Λ_α is the regularization scale.

For the direct two-to-two particle interaction, we introduce the separable potentials for the $N^*(1535)$ and $N^*(1440)$. For the $N^*(1535)$, only $\pi N \rightarrow \pi N$ interaction is applying,

$$V_{\pi N, \pi N}^S(k, k') = \frac{3g_{\pi N, \pi N}^{N^*(1535)} \tilde{u}_\alpha(k) \tilde{u}_{\pi N}(k')}{4\pi^2 f^2} \quad (7)$$

where $\tilde{u}_{\pi N}(k) = u(k)(m_\pi + \omega_\pi(k))/\omega_\pi(k)$ and $u(k)$ is the dipole form used in the G_{α, B_0} coupling. For the $N^*(1440)$,

$$V_{\alpha, \beta}^S(k, k') = g_{\alpha, \beta}^{N^*(1440)} \frac{\bar{G}_\alpha(k)}{\sqrt{\omega_{\alpha 1}(k)}} \frac{\bar{G}_\beta(k')}{\sqrt{\omega_{\beta 1}(k')}}}, \quad (8)$$

where $\bar{G}_\alpha(k) = G_{\alpha, B_0}(k)/g_{B_0\alpha}$. For $\Lambda^*(1405)$, we use the Weinberg-Tomozawa term [27] as follows:

$$V_{\alpha, \beta}^S(k, k') = g_{\alpha, \beta}^{\Lambda^*(1405)} \frac{[\omega_{\alpha M}(k) + \omega_{\beta M}(k')] u(k) u(k')}{16\pi^2 f^2 \sqrt{\omega_{\alpha M}(k) \omega_{\beta M}(k')}}}, \quad (9)$$

where the form factor is same as that in the vertex between bare particle and two-particle channels.

2.2 Infinite-Volume scattering amplitude

The T -matrices for two particle scattering are obtained by solving a three-dimensional reduction of the coupled-channel Bethe-Salpeter equations for each partial wave

$$t_{\alpha, \beta}(k, k'; E) = V_{\alpha, \beta}(k, k'; E) + \sum_\gamma \int q^2 dq \times \frac{V_{\alpha, \gamma}(k, q; E) t_{\gamma, \beta}(q, k'; E)}{E - \omega_{\gamma 1}(q) - \omega_{\gamma 2}(q) + i\epsilon}.$$

The coupled-channel potential is readily calculated from the interaction Hamiltonian

$$V_{\alpha, \beta}(k, k') = \sum_{B_0} \frac{G_{\alpha, B_0}^\dagger(k) G_{\beta, B_0}(k')}{E - m_{B_0}^0} + V_{\alpha, \beta}^S(k, k'), \quad (10)$$

with the normalization $\langle \alpha(\mathbf{k}) | \beta(\mathbf{k}') \rangle = \delta_{\alpha,\beta} \delta(\mathbf{k} - \mathbf{k}')$.

Finally, the S-matrix is related to the T -matrix by

$$S_{\alpha,\beta}(E) = 1 - 2i \sqrt{\rho_\alpha(E)\rho_\beta(E)} t_{\alpha,\beta}(k_{\alpha\text{ cm}}, k_{\beta\text{ cm}}; E), \quad (11)$$

$$\rho_\alpha(E) = \pi \frac{\omega_{\alpha_M\text{ cm}} \omega_{\alpha_N\text{ cm}}}{E} k_{\alpha\text{ cm}}, \quad (12)$$

where $k_{\alpha\text{ cm}}$ satisfies the on-shell condition $\omega_{\alpha_M\text{ cm}} + \omega_{\alpha_N\text{ cm}} = E$, and $\omega_{\alpha_i\text{ cm}} = \omega_{\alpha_i}(k_{\text{cm}})$.

The pole position of any bound state or resonance is obtained by searching for the poles of the T -matrix in the complex plane.

The cross section $\sigma_{\alpha,\beta}$ for the process $\alpha \rightarrow \beta$ is

$$\sigma_{\alpha,\beta} = \frac{4\pi^3 k_{\alpha\text{ cm}} \omega_{\alpha_M\text{ cm}} \omega_{\alpha_N\text{ cm}} \omega_{\beta_M\text{ cm}} \omega_{\beta_N\text{ cm}}}{E^2 k_{\beta\text{ cm}}} |t_{\alpha,\beta}(k_{\alpha\text{ cm}}, k_{\beta\text{ cm}}; E)|^2. \quad (13)$$

2.3 The Finite-Volume Matrix Hamiltonian

The formalism of the finite-volume matrix Hamiltonian is presented by following Refs.[17,18]. We can discretise the Hamiltonian in a box with length L . A particle can only carry momenta $k_n = \sqrt{n} 2\pi/L$ in the box, where $n = 0, 1, \dots$. The Hamiltonian in the finite-volume is the momentum discretization of the Hamiltonian H at infinite volume. Therefore, Eq. (1) can be extended in the finite-volume as:

$$H^V = H_0^V + H_I^V = H_0^V + g^V + v^V, \quad (14)$$

$$H_0^V = \sum_{B_0} |B_0\rangle m_B^0 \langle B_0| + \sum_n \sum_\alpha |\alpha(k_n)\rangle_V [\omega_{\alpha_M}(k_n) + \omega_{\alpha_N}(k_n)]_V \langle \alpha(k_n)|, \quad (15)$$

$$g^V = \sum_n \sum_{\alpha, B_0} \sqrt{\frac{C_3(n)}{4\pi}} \left(\frac{2\pi}{L}\right)^{3/2} \left\{ |\alpha(k_n)\rangle_V G_{\alpha, B_0}^\dagger(k_n) \langle B_0| + h.c. \right\}, \quad (16)$$

$$v^V = \sum_{n, n'} \sum_{\alpha, \beta} \sqrt{\frac{C_3(n) C_3(n')}{16\pi^2}} \left(\frac{2\pi}{L}\right)^3 |\alpha(k_n)\rangle_V V_{\alpha, \beta}^S(k_n, k_{n'})_V \langle \beta(k_{n'})|. \quad (17)$$

Here, $C_3(n)$ represents the number of ways of summing the squares of three integers to equal n . The normalization of $|\alpha(k_n)\rangle_V$ becomes ${}_V \langle \alpha(k_n) | \beta(k_{n'}) \rangle_V = \delta_{nn'} \delta_{\alpha\beta}$. Then it is straightforward to get the matrix of Hamiltonian in the finite-volume. One can obtain the eigenstate energy levels on the lattice and analyse the corresponding eigenvector wave functions describing the constituents of the eigenstates with the finite-volume Hamiltonian matrix.

In addition to the results at physical pion mass, we can also extend the formalism to unphysical pion masses. Using m_π^2 as a measure of the light quark

masses, we consider the variation of the bare (B_0) mass and meson (M) mass as:

$$m_B^0(m_\pi^2) = m_B^0|_{\text{phy}} + \alpha_{B_0} (m_\pi^2 - m_\pi^2|_{\text{phy}}), \quad (18)$$

$$m_M^2(m_\pi^2) = m_M^2|_{\text{phy}} + \alpha_M (m_\pi^2 - m_\pi^2|_{\text{phy}}), \quad (19)$$

where the slope parameters α_{B_0} for bare states are constrained by lattice QCD data from the CSSM. The stable particles such as N , Δ , Σ and K use linear interpolations between the corresponding lattice QCD results. For the σ , it uses $\alpha_\sigma = \frac{4}{3}m_\sigma|_{\text{phy}}\alpha_N = 0.67[28]$, where $\alpha_N = 1.0 \text{ GeV}^{-1}$. The slope parameter of the η meson is used $\frac{1}{3}$.

2.4 The relationship between the eigenstate and the resonance

The main difference between finite and infinite volume in the momentum space is the discretization of the momentum in the box. It leads to the discrete eigenvalue of the Hamiltonian matrix. Therefore, the eigenstates in the box are the discrete states of the continuum final scattering states in the infinite-volume. Each eigenstate can not be recognized as a resonance directly, while the resonance is recognized as a pole position on the complex plan of the scattering amplitude. As we known, the resonance will make enhancement of the cross-section, i.e., the bump on the figures of cross-section vs scattering energy. In other words, when we find one peak of cross-section vs total energy, sometimes it may exists a resonance around this energy. Around one peak, there are infinite final scattering states, the behavior of resonance at the real axis is taken by these states. In other words, the pole position on the complex plan will be shown as a peak on the real axis. Such resonance peak can be also observed by the overlap between bare state and final scattering state, as shown the red color line in Fig.1. Correspondingly, the overlap between bare state and eigenstate of finite volume also can be used to find such peak for resonance. Based on Ref. [24], we define two variables P^V and P for finite and infinite volume, respectively,

$$P^V(E_k^{ave}, L) = \frac{1}{Z^V} \frac{1}{\Delta E} \sum_{E_k^{ave} - \frac{\Delta E}{2} \leq E_i \leq E_k^{ave} + \frac{\Delta E}{2}} |\langle B_0 | \Psi_{E_i}^V \rangle|^2, \quad (20)$$

$$P(E) = \frac{1}{Z} \sum_{\alpha} \pi k_{\alpha \text{ cm}} \omega_{\alpha M \text{ cm}} \omega_{\alpha B \text{ cm}} |\langle B_0 | \Psi_{E,\alpha}^{(+)} \rangle|^2, \quad (21)$$

where Z^V and Z are the normalization factors, and $|\Psi_{E,\alpha}^{(+)}\rangle$ and $|\Psi_{E_i}^V\rangle$ are the final scattering states of channel α in the infinite-volume and i -th finite-volume eigenstates, respectively.

As an example, we use the Sato-Lee model [29,30,31] to calculate the Hamiltonian including the bare Δ state and πN channel. The eigenstates in the finite-volume are solved from the eigen-equation of the Hamiltonian matrix,

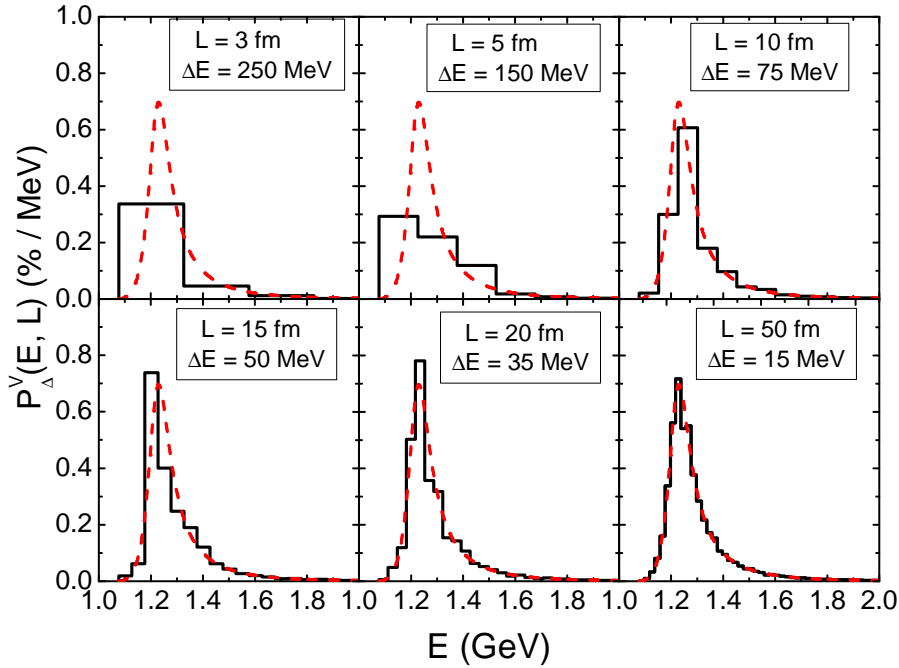


Fig. 1 The probability $P^V(E, L)$ (black solid line) and $P(E)$ (red dashed curve) of the Sato-Lee model model at the $\Delta(1232)$ energy region with $L = 3, 5, 10, 15, 20,$ and 50 fm.

while the final scattering states are calculated by the T-matrix in the infinite-volume. Finally, we show the black solid and red dashed lines for the P^V and P defined in Eq.(20, 21). The Δ resonance peak is very clean. This diagram does not show the relationship between the eigenstate of finite-volume and the resonance, but also shows that the P^V agrees very well with P when L goes to infinite. Furthermore, for the small lattice size, you can find there are only several eigenstates around the peak area, it suggests that these states reflect the properties of the resonance. Thus, the complements of these eigenstates should reflect the inside structure of resonance.

Unfortunately, current Lattice techniques can not measure all eigenstates and eigenvectors for baryon resonances. At present, for the Baryon spectrum, pure three-quark local operators are mostly used. Through these operators, we still can have a glance of the inside structure of the excited nucleons. Overlap with the meson baryon scattering states is suppressed by factor of thousand relative to the nucleon. Therefore, the three-quark operator excites the bare state of the Hamiltonian model. The eigenstates seen on the lattice should have large bare state components.

2.5 The approach of HEFT

We briefly introduce the approach of HEFT as follows:

- 1 Fitting experimental data to fix the parameters of the interaction Hamiltonian.
- 2 Using these fitted parameters to generate the Finite-Volume Hamiltonian matrix. And for high pion mass, another parameter for the mass slope is needed.
- 3 Calculate the eigenvalue and eigenvector of this matrix to compare with Lattice data.

3 Results

In this section, we review the main results of the $N^*(1535)$, $\Lambda^*(1405)$ and $N^*(1440)$ resonances by using HEFT.

3.1 For $N^*(1535)$

With the excellent fit of phase shift and inelasticity of $\pi N \rightarrow \pi N$ around the $N^*(1535)$ region, the parameters $g_{B,\pi N}$, $g_{B,\eta N}$ and $g_{\pi N,\pi N}$ in the Hamiltonian are fixed. The fits of phase shift and inelasticity are shown in Fig.2. Then the bare mass slope is fixed by fitting various lattice QCD data, and we get the spectra with $L \sim 2$ and 3 fm, as shown in Fig.3. The values of fitted parameters are listed in Ref. [19]. Furthermore, it also shows the three eigenstates with largest bare state components as red, blue and green colors. The lattice QCD data following the color lines is well consistent with the assumption that three-quark operators couple most strongly to this bare state component. It indicates that our explanation based on HEFT agrees with lattice QCD results. Typically, the Hamiltonian eigenstates around 1535 MeV at the physical π mass region are dominated by bare-state contributions. It reflects that the main component of $N^*(1535)$ is the bare state, i.e., three-quark core. Therefore, the $N^*(1535)$ as the first negative-parity excitation of the nucleon, almost 600 MeV higher in mass is following the expectation based upon the harmonic oscillator model. We should point out it does not mean $N^*(1535)$ is a pure three-quark state, from our calculation, the fourth eigenstate also includes the components from πN and ηN scattering state. But that is no doubt that $N^*(1535)$ is dominated by the three-quark state.

3.2 For $\Lambda^*(1405)$

For the $\Lambda^*(1405)$ case, the cross sections of various channels are fitted as shown in Fig.4. Here, two different models with and without bare state are developed.

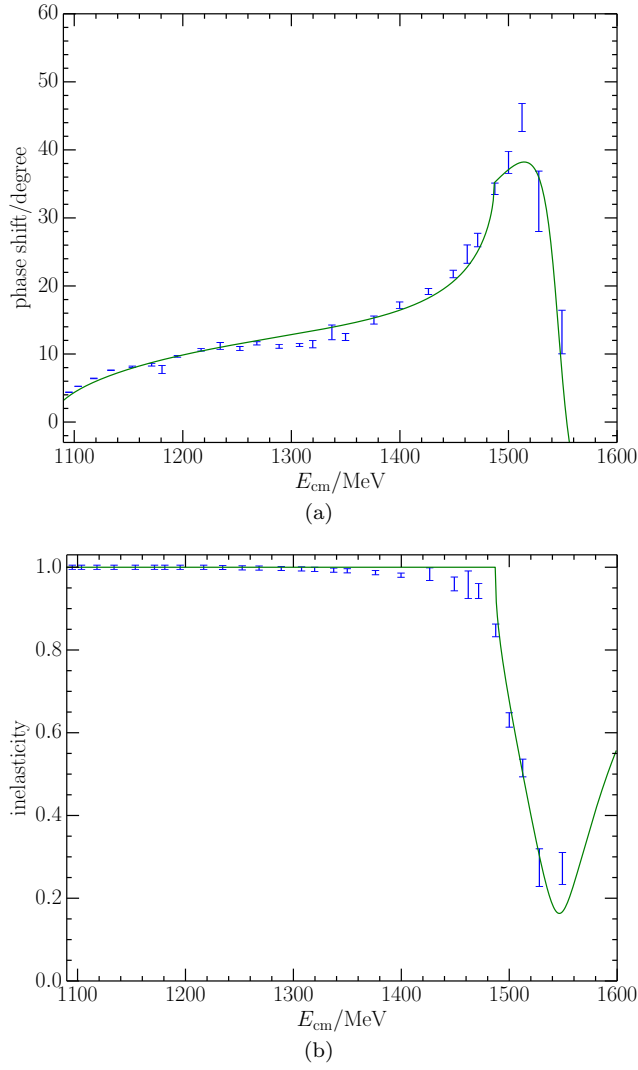


Fig. 2 Colour online: Experimental data for the phase shift (a) and inelasticity (b) for πN scattering with $J^P = 1/2^-$ are fit by the Hamiltonian model.

The fitted parameters values are shown in Ref. [22]. The corresponding two spectra are shown in Fig.5. Furthermore, the various components of second and fourth eigenstates of the finite-volume Hamiltonian matrix are shown in Fig.6. It is clear that the two lattice QCD points at the largest π mass can be only explained by the model with bare state. However, it is interesting to notice that at the physical π mass region, even in the with bare state model, the second eigenstate around 1405 MeV just takes around 5% bare state components. The components of the second eigenstate in the two models are both dominated by

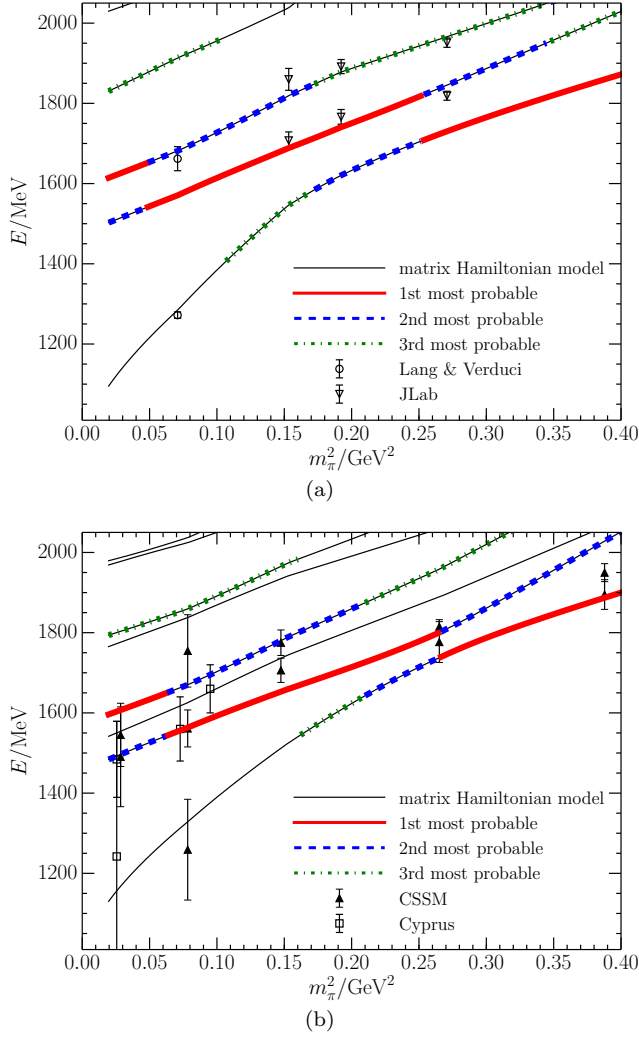


Fig. 3 Colour online: The pion mass dependence of the $L \simeq 1.98$ fm (a) and $L \simeq 2.90$ fm (b) finite-volume energy eigenstates. The different line types and colours indicate the strength of the bare basis state in the Hamiltonian-model eigenvector. The lattice QCD data are from Jlab [32,33], Lang & Verduci [34], CSSM [35,36,37] and Cyprus [38].

$\bar{K}N$ components as shown in Fig.6. It is confirmed that the main components of $\Lambda^*(1405)$ is the $\bar{K}N$. This result indicates that $\Lambda^*(1405)$ can not be recognize as a three-quark state, while it is better to be described as a bound state of $\bar{K}N$ near the physical pion mass. It is worthwhile to point out that the fourth eigenstate, having the largest bare state component is above 1600 MeV. It is also consistent with the prediction of the harmonic oscillator model for the first excitation of Λ resonance.

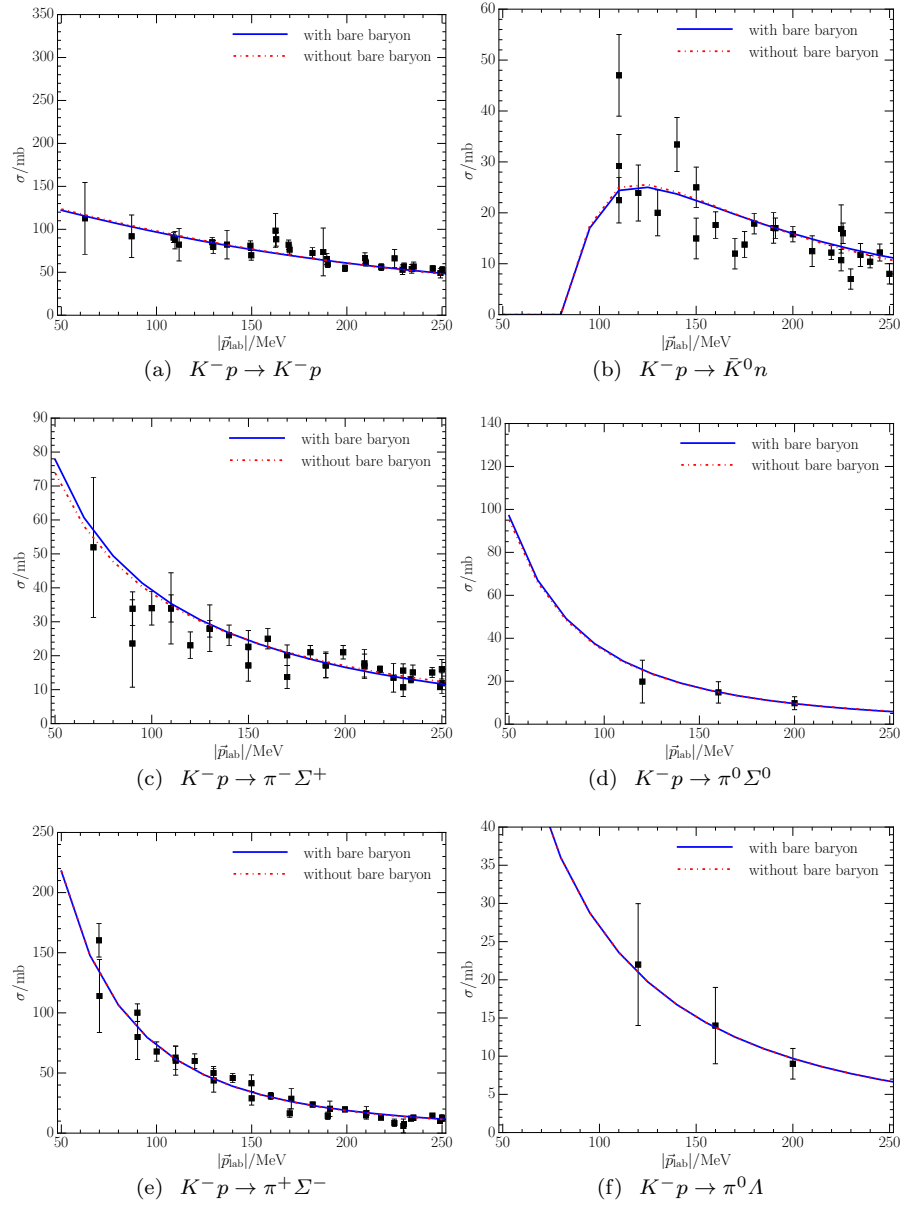


Fig. 4 Experimental data and our fits to the cross sections of K^-p . The solid lines are for our scenario with a bare-baryon component included in the $I = 0$ channel, and the dashed lines represent the results without a bare-baryon component. The experimental data are from Refs. [40, 41, 42, 43, 44, 45, 46].

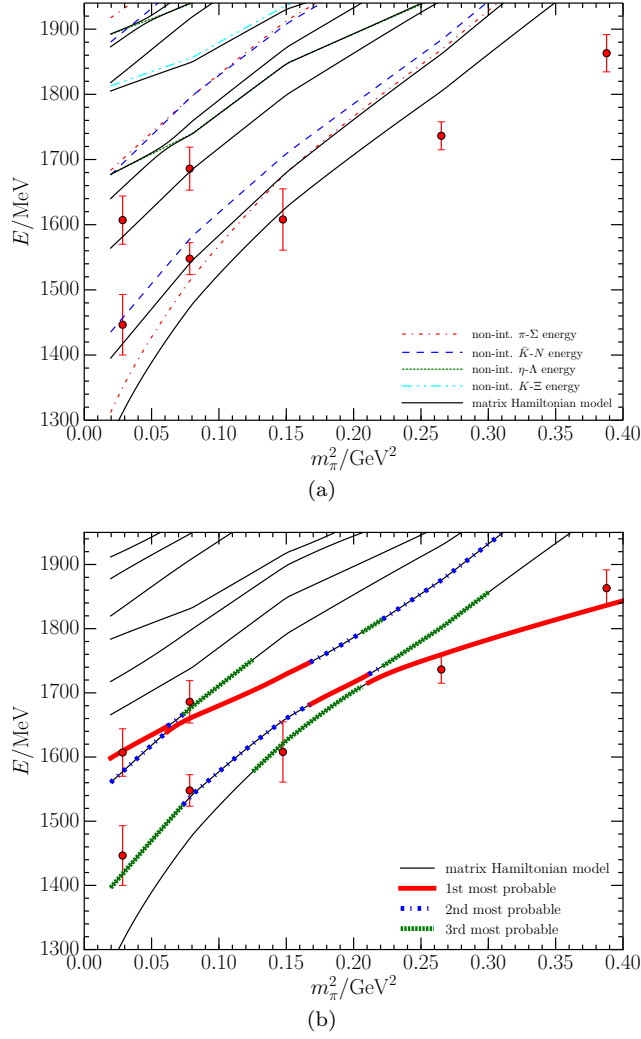


Fig. 5 Colour online: The pion-mass dependence of the finite-volume energy eigenstates for the scenario without (a) and with (b) a bare-baryon basis state. The broken lines represent the non-interacting meson-baryon energies and the solid lines represent the spectrum derived from the matrix Hamiltonian model. The thick-solid (red), dashed (blue) and short-dashed (green) lines correspond to the first, second, and third strongest bare-state contributions, and therefore the most likely states to be observed with three-quark interpolating fields. The lattice QCD results are from the CSSM [20, 47].

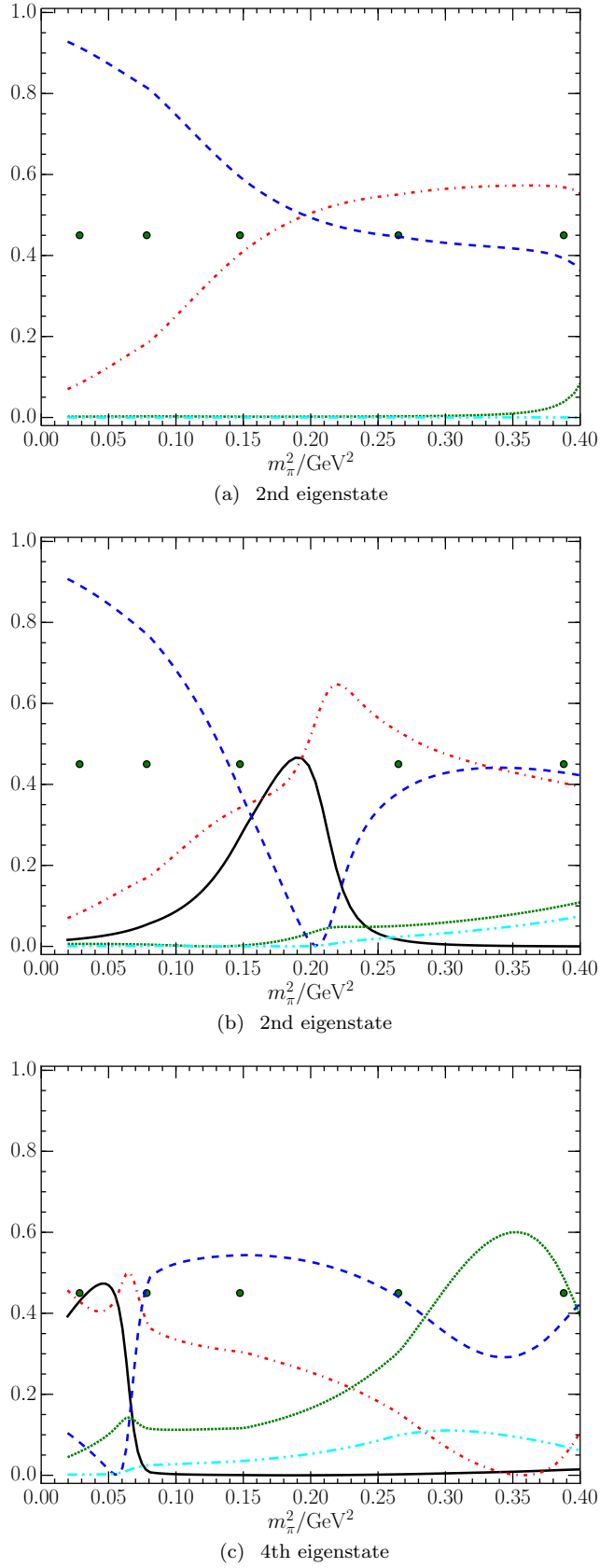


Fig. 6 Colour online: The pion-mass evolution of the Hamiltonian eigenvector components for the eigenstates observed in the scenario. The (a) and (b) are for the second eigenstate without and with bare state scenario. The (c) is for the fourth eigenstate with bare state scenario. The black solid, red dot-dashed, blue dashed, green dotted and cyan dot-dot-dashed lines are for bare state, $|\pi N\rangle$, $|\bar{K}N\rangle$, $|\eta A\rangle$ and $|K \Xi\rangle$, respectively. The (green) dots plotted horizontally at $y = 0.45$ indicate the positions of the five quark masses considered by the CSSM on a lattice volume with $L \simeq 2.90$ fm.

3.3 For $N^*(1440)$

There is a long puzzle for the nature of the Roper, $N^*(1440)$. By a similar method as that applied for the $N^*(1535)$ and $\Lambda^*(1405)$ resonances, the $N^*(1440)$ is studied with the experimental data and recent lattice QCD results. The fitted phase shift, inelasticity and T-matrix for $\pi N \rightarrow \pi N$ are shown in Fig.7. We find two rather different models which appear equally acceptable in terms of the quality of the fit to existing data, as red-solid and blue-dashed lines in Fig.7. The values of parameters are listed in Ref. [23]. The main differences between these two models are the coupling of $\pi N \rightarrow \pi N$ in scenario I is much larger than another, while the coupling of the bare state to πN and σN in scenario I is much smaller. These differences leads two pictures of the Roper, it is generated by the strong rescattering in the baryon-meson channels or dominated by the bare state.

Through HEFT approach, two spectra in the finite volume are shown in Fig.8. The predictions of scenario I are consistent with lattice QCD because all of the lattice states dominated by local three-quark interpolating fields can be associated with a colored line. For example, all of the Hamiltonian states having the largest bare basis-state component, indicated in red in Fig. 8, have a nearby lattice QCD result. On the other hand, scenario II displays little correspondence to the lattice QCD results. Scenario II predicts a low-lying state with a large bare basis-state component of approximately 50%, approaching that for the ground state. Such a state would be easy to excite in lattice QCD with local three-quark operators. However this state is not seen in the simulations through the local three-quark operators. Indeed, Lang *et al.* [26] only see this state when they include a non-local πN interpolating field. Obviously, scenario II fails to explain lattice data. Furthermore, the lowest two states observed by the Lang *et al.* group are quite consistent with scenario I. Near the physical mass the first eigenstate is dominated by σN basis states, while the main components of the second state is πN basis states. The Lang group find only the first and second state when they include a non-local σN and πN interpolating field, respectively. From this study of the Roper, the mystery of the low-lying Roper resonance may be nearing resolution. Evidence indicates the observed nucleon resonance at 1440 MeV is best described as the result of strong rescattering between coupled meson-baryon channels. And the excited state from three-quark core is around 1.9 GeV, which is consistent with the harmonic oscillator model.

3.4 The picture of the lowest N^* and Λ^*

Through HEFT to study of $N^*(1535)$, $\Lambda^*(1405)$ and $N^*(1440)$, the nature of these resonance states is found as follows:

- 1 For $N^*(1535)$, it is mainly dominated by a three-quark core.

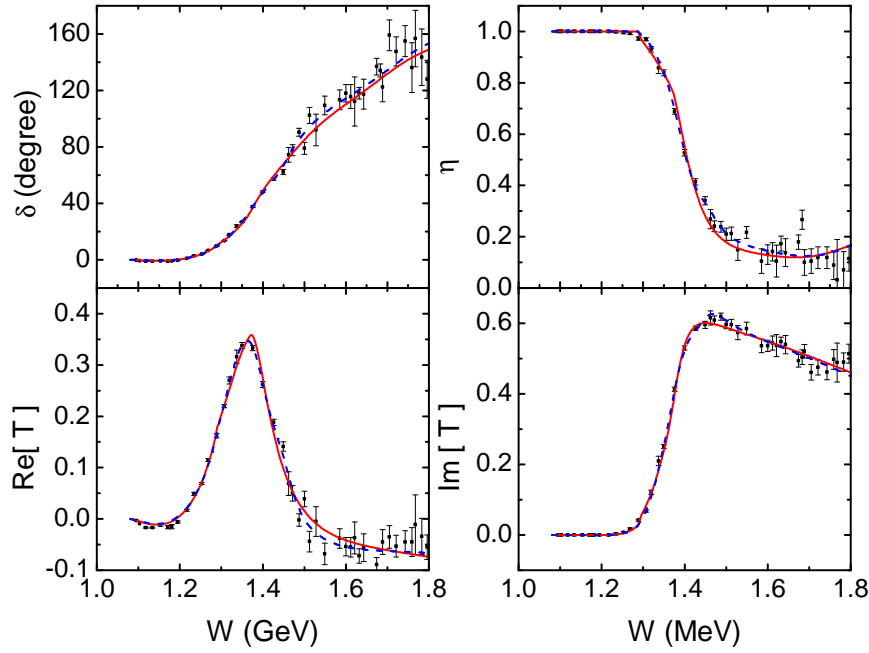


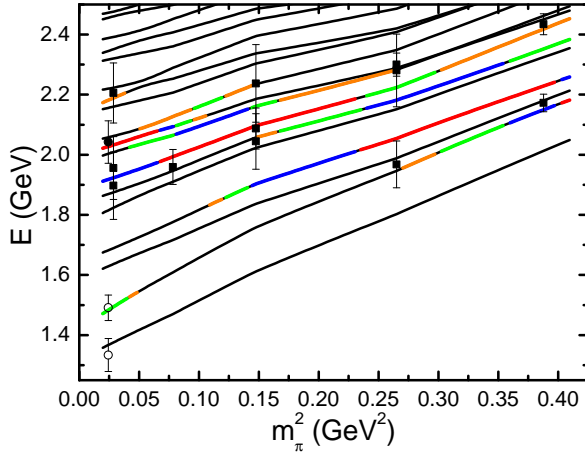
Fig. 7 The fitted phase shift δ , inelasticity η and T -matrix for the $\pi N \rightarrow \pi N$ reaction. Red-solid and blue-dashed lines are calculated from scenarios I and II, respectively.

- 2 For $\Lambda^*(1405)$, it is predominantly a molecular $\bar{K}N$ bound state. The excited state of the quark model is around 1.6 GeV.
- 3 For $N^*(1440)$, it is best described as the result of strong rescattering between coupled meson-baryon channels. The first radial excited nucleon of the quark model is around 1.9 GeV.

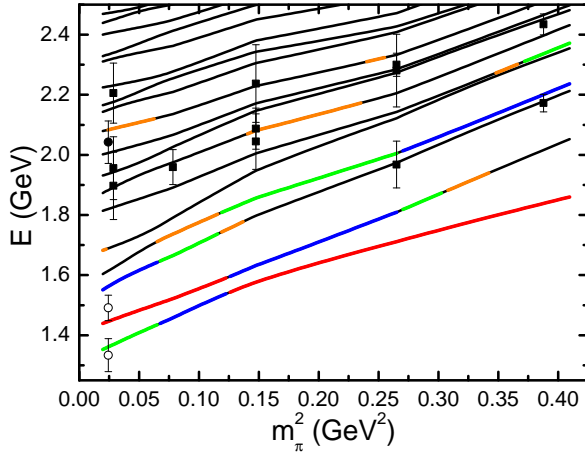
These conclusions lead to the new picture of low lying N and Λ resonances as shown in Fig.9. From the quark model, it predicts three levels of hadron mass. However, from the experimental data, $\Lambda^*(1405)$ and $N^*(1440)$ do not obey this mass order. Through the analyses of Lattice QCD results based on HEFT, the nature of $\Lambda^*(1405)$ and $N^*(1440)$ are predominantly meson-baryon states, rather than three-quark states. In other words, these two states are beyond the quark model. On the other hand, the states predicted in the quark model all have evidence from the analyses of lattice QCD results.

4 Conclusion

In this report, HEFT approach is introduced. HEFT connects the experimental data, Lattice QCD results and the properties of resonances. From the



(a)



(b)

Fig. 8 The finite volume spectrum of Scenario I(a) with a bare mass of 2.0 GeV and Scenario II(b) having a bare mass of 1.7 GeV. The CSSM results [21] are indicated by square symbols and circles denote the more recent results from Lang *et al.* [26]. Solid symbols indicate states dominated by local three-quark operators and open symbols indicate states dominated by non-local momentum-projected five-quark operators. The colours red, blue, green and orange are used to indicate the relative contributions of the bare baryon basis state in the eigenstate, with red being the largest contribution.

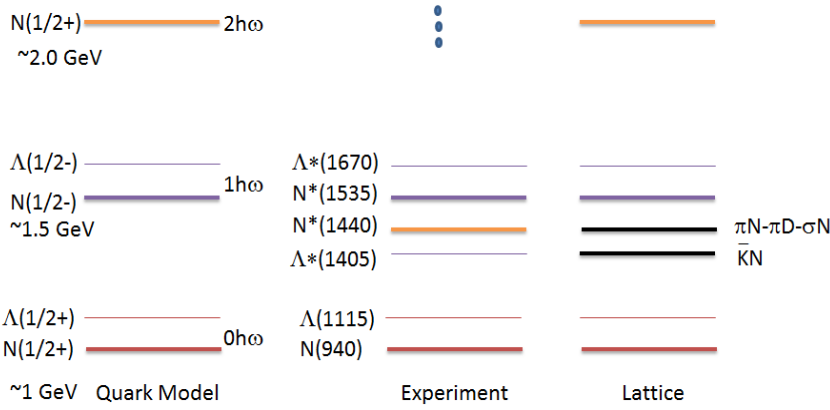


Fig. 9 The spectra of N and Λ of the quark model, experimental data and the analysis of this paper.

Hamiltonian matrix in the finite-volume, it does not only get the eigenvalues which corresponding to the spectrum of Lattice QCD simulation, but also provides the eigenvectors of these eigenstates. The eigenvectors will be useful to distinguish the different models and reflect the insight of the resonances. The $N^*(1535)$, $\Lambda^*(1405)$ and $N^*(1440)$ are studied based on HEFT combined with experimental and lattice QCD data. The lattice QCD data show that the $\Lambda^*(1405)$ and $N^*(1440)$ are dominated by the meson-baryon interaction, while the $N^*(1535)$ is mainly composed of three-quarks. Furthermore, from lattice QCD data, there is evidence to show that the first excited state of the Λ is around 1.6 GeV, and the first radial excited state of nucleon is around 1.9 GeV. All of above conclusions show that the states found in the lattice QCD results are consistent with the expectations of the harmonic oscillator model, except $\Lambda^*(1405)$ and $N^*(1440)$.

The definitive analysis for the picture of hadron needs new data to further resolve the nature of these resonance states. It requires new experimental data and lattice QCD simulations, especially, also complete nucleon spectrum on several lattice volumes.

References

1. D. Mohler, “Recent results on the meson and baryon spectrum from lattice QCD,” EPJ Web Conf. **137**, 05018 (2017)
2. M. Luscher, “Volume Dependence of the Energy Spectrum in Massive Quantum Field Theories. 2. Scattering States,” Commun. Math. Phys. **105**, 153 (1986).
3. M. Luscher, “Two particle states on a torus and their relation to the scattering matrix,” Nucl. Phys. B **354**, 531 (1991).
4. K. Rummukainen and S. A. Gottlieb, “Resonance scattering phase shifts on a nonrest frame lattice,” Nucl. Phys. B **450**, 397 (1995)
5. C. h. Kim, C. T. Sachrajda and S. R. Sharpe, “Finite-volume effects for two-hadron states in moving frames,” Nucl. Phys. B **727**, 218 (2005)

6. S. He, X. Feng and C. Liu, “Two particle states and the S-matrix elements in multi-channel scattering,” JHEP **0507**, 011 (2005)
7. M. T. Hansen and S. R. Sharpe, “Multiple-channel generalization of Lellouch-Luscher formula,” Phys. Rev. D **86**, 016007 (2012)
8. R. A. Briceno, Z. Davoudi and T. C. Luu, “Two-Nucleon Systems in a Finite Volume: (I) Quantization Conditions,” Phys. Rev. D **88**, no. 3, 034502 (2013)
9. M. Gockeler, R. Horsley, M. Lage, U.-G. Meissner, P. E. L. Rakow, A. Rusetsky, G. Schierholz and J. M. Zanotti, “Scattering phases for meson and baryon resonances on general moving-frame lattices,” Phys. Rev. D **86**, 094513 (2012)
10. R. A. Briceno, “Two-particle multichannel systems in a finite volume with arbitrary spin,” Phys. Rev. D **89**, no. 7, 074507 (2014)
11. M. Doring, U. G. Meissner, E. Oset and A. Rusetsky, “Unitarized Chiral Perturbation Theory in a finite volume: Scalar meson sector,” Eur. Phys. J. A **47**, 139 (2011)
12. M. Doring, U. G. Meissner, E. Oset and A. Rusetsky, “Scalar mesons moving in a finite volume and the role of partial wave mixing,” Eur. Phys. J. A **48**, 114 (2012)
13. A. Martinez Torres, L. R. Dai, C. Koren, D. Jido and E. Oset, “The KD , ηD_s interaction in finite volume and the nature of the $D_{s^*0}(2317)$ resonance,” Phys. Rev. D **85**, 014027 (2012)
14. M. Doring and U. G. Meissner, “Finite volume effects in pion-kaon scattering and reconstruction of the $\kappa(800)$ resonance,” JHEP **1201**, 009 (2012)
15. M. Doring, M. Mai and U. G. Meissner, “Finite volume effects and quark mass dependence of the $N(1535)$ and $N(1650)$,” Phys. Lett. B **722**, 185 (2013)
16. L. S. Geng, X. L. Ren, Y. Zhou, H. X. Chen and E. Oset, “S-wave KK^* interactions in a finite volume and the $f_1(1285)$,” Phys. Rev. D **92**, no. 1, 014029 (2015)
17. J. M. M. Hall, A. C.-P. Hsu, D. B. Leinweber, A. W. Thomas and R. D. Young, “Finite-volume matrix Hamiltonian model for a $\Delta \rightarrow N\pi$ system,” Phys. Rev. D **87**, no. 9, 094510 (2013)
18. J. J. Wu, T.-S. H. Lee, A. W. Thomas and R. D. Young, “Finite-volume Hamiltonian method for coupled-channels interactions in lattice QCD,” Phys. Rev. C **90**, no. 5, 055206 (2014)
19. Z. W. Liu, W. Kamleh, D. B. Leinweber, F. M. Stokes, A. W. Thomas and J. J. Wu, “Hamiltonian effective field theory study of the $N^*(1535)$ resonance in lattice QCD,” Phys. Rev. Lett. **116**, no. 8, 082004 (2016)
20. J. M. M. Hall, W. Kamleh, D. B. Leinweber, B. J. Menadue, B. J. Owen, A. W. Thomas and R. D. Young, “Lattice QCD Evidence that the (1405) Resonance is an Antikaon-Nucleon Molecule,” Phys. Rev. Lett. **114**, no. 13, 132002 (2015)
21. Z. W. Liu, W. Kamleh, D. B. Leinweber, F. M. Stokes, A. W. Thomas and J. J. Wu, “Hamiltonian effective field theory study of the $N^*(1440)$ resonance in lattice QCD,” Phys. Rev. D **95**, no. 3, 034034 (2017)
22. Z. W. Liu, J. M. M. Hall, D. B. Leinweber, A. W. Thomas and J. J. Wu, “Structure of the $\Lambda(1405)$ from Hamiltonian effective field theory,” Phys. Rev. D **95**, no. 1, 014506 (2017)
23. J. j. Wu, D. B. Leinweber, Z. w. Liu and A. W. Thomas, “Structure of the Roper Resonance from Lattice QCD Constraints,” arXiv:1703.10715 [nucl-th] (2017).
24. J. J. Wu, H. Kamano, T.-S. H. Lee, D. B. Leinweber and A. W. Thomas, “Nucleon resonance structure in the finite volume of lattice QCD,” Phys. Rev. D **95**, no. 11, 114507 (2017)
25. R. D. Young, D. B. Leinweber and A. W. Thomas, “Convergence of chiral effective field theory,” Prog. Part. Nucl. Phys. **50**, 399 (2003)
26. C. B. Lang, L. Leskovec, M. Padmanath and S. Prelovsek, “Pion-nucleon scattering in the Roper channel from lattice QCD,” Phys. Rev. D **95**, no. 1, 014510 (2017)
27. E. A. Veit, A. W. Thomas and B. K. Jennings, “ KN Scattering in the Cloudy Bag Model: s , p and d Waves,” Phys. Rev. D **31**, 2242 (1985).
28. I. C. Cloet, D. B. Leinweber and A. W. Thomas, “Simple quark model with chiral phenomenology,” Phys. Rev. C **65**, 062201 (2002)
29. T. Sato and T. S. H. Lee, “Meson exchange model for πN scattering and $\gamma N \rightarrow \pi N$ reaction,” Phys. Rev. C **54**, 2660 (1996)
30. T. Sato and T. S. H. Lee, “Dynamical study of the Delta excitation in N (e , e' - π) reactions,” Phys. Rev. C **63**, 055201 (2001)

31. B. Julia-Diaz, T.-S. H. Lee, T. Sato and L. C. Smith, "Extraction and Interpretation of gamma N \rightarrow Δ Form Factors within a Dynamical Model," *Phys. Rev. C* **75**, 015205 (2007)
32. R. G. Edwards, J. J. Dudek, D. G. Richards and S. J. Wallace, "Excited state baryon spectroscopy from lattice QCD," *Phys. Rev. D* **84**, 074508 (2011)
33. R. G. Edwards *et al.* [Hadron Spectrum Collaboration], "Flavor structure of the excited baryon spectra from lattice QCD," *Phys. Rev. D* **87**, no. 5, 054506 (2013)
34. C. B. Lang and V. Verduci, "Scattering in the N negative parity channel in lattice QCD," *Phys. Rev. D* **87**, no. 5, 054502 (2013)
35. A. L. Kiratidis, W. Kamleh, D. B. Leinweber and B. J. Owen, "Lattice baryon spectroscopy with multi-particle interpolators," *Phys. Rev. D* **91**, 094509 (2015)
36. M. S. Mahub, W. Kamleh, D. B. Leinweber, P. J. Moran and A. G. Williams, "Structure and Flow of the Nucleon Eigenstates in Lattice QCD," *Phys. Rev. D* **87**, no. 9, 094506 (2013)
37. M. S. Mahub, W. Kamleh, D. B. Leinweber, P. J. Moran and A. G. Williams, "Low-lying Odd-parity States of the Nucleon in Lattice QCD," *Phys. Rev. D* **87**, no. 1, 011501 (2013)
38. C. Alexandrou, T. Leontiou, C. N. Papanicolas and E. Stiliaris, "Novel analysis method for excited states in lattice QCD: The nucleon case," *Phys. Rev. D* **91**, no. 1, 014506 (2015)
39. G. S. Abrams and B. Sechi-Zorn, "Charge-Exchange Scattering of Low-Energy K-Mesons in Hydrogen," *Phys. Rev.* **139**, B454 (1965).
40. M. Sakitt, T. B. Day, R. G. Glasser, N. Seeman, J. H. Friedman, W. E. Humphrey and R. R. Ross, "Low-energy K- Meson Interactions In Hydrogen," *Phys. Rev.* **139**, B719 (1965).
41. J. K. Kim, "Low Energy K- p Interaction of the 1405 MeV Y^*0 Resonance as $K\bar{b}N$ Bound State," *Phys. Rev. Lett.* **14**, 29 (1965).
42. M. Csejthey-Barth *et al.*, "The interactions of low energy K^- mesons with protons," *Phys. Lett.* **16**, 89 (1965).
43. T. S. Mast, M. Alston-Garnjost, R. O. Bangerter, A. S. Barbaro-Galtieri, F. T. Solmitz and R. D. Tripp, *Phys. Rev. D* **14**, 13 (1976). doi:10.1103/PhysRevD.14.13
44. R. O. Bangerter, M. Alston-Garnjost, A. Barbaro-Galtieri, T. S. Mast, F. T. Solmitz and R. D. Tripp, "Reactions $K^-p \rightarrow \Sigma^- \pi^+$ and $K^-p \rightarrow \Sigma^+ \pi^-$ in the Momentum Range From 220-MeV/c to 470-MeV/c," *Phys. Rev. D* **23**, 1484 (1981).
45. J. Ciborowski *et al.*, *J. Phys. G* **8**, 13 (1982). doi:10.1088/0305-4616/8/1/005
46. D. Evans, J. V. Major, E. Rondio, J. A. Zakrzewski, J. E. Conboy, D. J. Miller and T. Tymieniecka, "Charge Exchange Scattering In K- P Interactions Below 300-mev/c," *J. Phys. G* **9**, 885 (1983).
47. B. J. Menadue, W. Kamleh, D. B. Leinweber and M. S. Mahub, "Isolating the $\Lambda(1405)$ in Lattice QCD," *Phys. Rev. Lett.* **108**, 112001 (2012)